Molecular simulation and experiments of water adsorption in a high surface area activated carbon: Hysteresis, scanning curves and spatial organization of water clusters

Accepted Manuscript

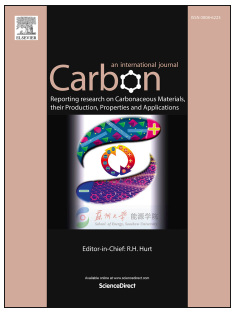

Molecular simulation and experiments of water adsorption in a high surface area activated carbon: Hysteresis, scanning curves and spatial organization of water clusters

Lev Sarkisov, Alessio Centineo, Stefano Brandani

PII: S0008-6223(17)30285-3

DOI: 10.1016/j.carbon.2017.03.044

Reference: CARBON 11851

To appear in: *Carbon*

Received Date: 16 January 2017

Revised Date: 11 March 2017

Accepted Date: 13 March 2017

Please cite this article as: L. Sarkisov, A. Centineo, S. Brandani, Molecular simulation and experiments of water adsorption in a high surface area activated carbon: Hysteresis, scanning curves and spatial organization of water clusters, *Carbon* (2017), doi: 10.1016/j.carbon.2017.03.044.

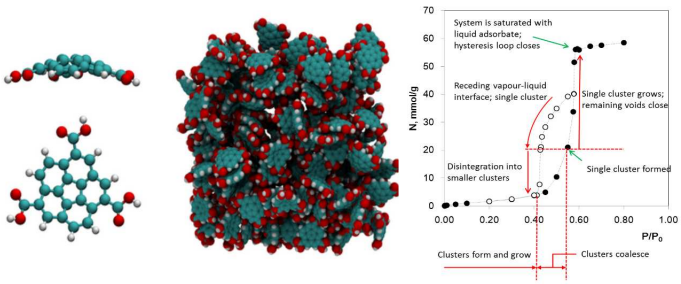

Molecular simulation and experiments of water adsorption in a high surface area activated carbon: hysteresis, scanning curves and spatial organization of water clusters

Lev Sarkisov[*]*, Alessio Centineo, Stefano Brandani*

Institute for Materials and Processes, School of Engineering, The University of Edinburgh, EH9 3JL, UK

Abstract. Despite decades of research, quantitatively accurate molecular models of water sorption on activated carbons remain elusive, while many phenomena are not properly understood even qualitatively. Here we focus specifically on scanning phenomena. Scanning isotherms, obtained by reversing either adsorption or desorption process before the closure of the hysteresis loop, have been recently explored as a sensitive experimental probe for structural characterization of activated carbons and at the same time have been subject of several competing theories of adsorption. We employ adsorption experiments and molecular simulations to understand the nature of the states along the adsorption and scanning curves for water at 308K in a high surface area activated carbon, Maxsorb. The molecular model considered here is based on a random packing of fullerene-like fragments, functionalized with carboxylate groups. The model is able to reproduce reasonably well the shape of the adsorption and scanning desorption isotherms. We investigate spatial organization, structure, size and interaction between the clusters on the adsorption branch. Furthermore, we show that the scanning desorption isotherm consists of a series of states of the system where a single cluster of water shrinks in size as water evaporates from its surface, before it finally disintegrates into separate smaller clusters.

[*] Corresponding author. Email: Lev.Sarkisov@ed.ac.uk

1. Introduction

Adsorption of water on activated carbons has been subject of numerous theoretical and experimental studies [1]. From the industrial perspective, presence of water vapour needs to be taken into account in many gas separation processes, including natural gas sweetening, carbon capture and volatile organic compounds removal from air streams. Design and optimization of these processes would significantly benefit from having accurate, predictive models of water adsorption in porous materials. Water adsorption has been also proposed as a method for characterization of oxygen groups on the surface of porous carbons [2-4], and as a general characterization method [5, 6], complementing the arsenal of more traditional physical adsorption characterization techniques based on nitrogen and argon adsorption at cryogenic conditions and carbon dioxide adsorption at 273K.

Furthermore, more recently, Velasco *et al.* attempted to link hysteresis and scanning sorption behaviour of water in activated carbons with the topology and surface chemistry of the material [7]. It emerges from this study that water scanning behaviour is sensitive to both surface chemistry and structure of the activated carbon, and in this capacity it could be seen as a promising technique for porous material characterization. The principal challenge, however, in the interpretation of the water adsorption hysteresis and scanning isotherms in activated carbons is lack of a molecular level description of the states of the system and confined water along these isotherms. This defines the remit of the current article: to develop a molecular model of an activated carbon capable of generating a reasonably realistic adsorption isotherm and scanning curves for water; and, using this model, to explore the nature and spatial organization of the adsorbed states along the scanning curves. For this we adopt a variant of a previously developed model of a high surface area activated carbon based on a random packing of fullerene-like fragments functionalized with oxygen edge groups [8, 9]. However, to justify selection of this model as a starting point in our endeavours, it is

instructive to briefly review the current state-of-the-art in theoretical studies of water adsorption in activated carbons.

Firstly, it is important to recognize that predictive, accurate molecular models of water adsorption in activated carbons remain largely elusive, although some promising directions started to emerge [10]. This situation stems from two principal challenges. The first challenge is associated with the very complex internal structure of activated carbons [11]. Construction of a molecular model of an activated carbon can be guided by the available data from neutron and X-ray scattering experiments, data on porosity and surface area, reference adsorption results used for model calibration; however there is no single and consistent strategy for this process and different approaches proposed over the years vary substantially in the effort required for their adoption and in the quality of the predicted adsorption data, even for light gases such as carbon dioxide and methane. This is in stark contrast with the field of zeolites, where, in the absence of ambiguity about the structure of the material, accurate models for adsorption for light gases, alkanes, aromatics and other species have been developed over the years (see for example, Ref [12-14]). The second challenge is associated with the very nature of the adsorbate itself. Many models of water have been proposed over the years [15, 16]. Yet, within the range of reasonably simple, transferrable and computationally tractable models (based on rigid structures and point charges), none of the models maintains consistent accuracy across the whole phase diagram [15]. Even at ambient conditions, accuracy of these models still needs substantial improvement in the prediction of bulk properties, such as saturated vapour pressure, let alone quantitative predictions of water adsorption. Not surprisingly, prediction of water adsorption has been very challenging for all types of materials, including the crystalline ones (see, for example, Ref [17]).

Although there is no quantitative molecular model of water adsorption in activated carbons, we do have a fairly good qualitative understanding of the processes. At low pressures, water

molecules associate with the individual polar surface groups; the water clusters initiated in this fashion grow in size and at some point start to coalesce with each other. Depending on the structure of the carbon material, this coalescence process may occur in several stages. This picture was originally proposed by Gubbins and co-workers using graphitic slit pores decorated with surface groups as a simple model of an activated carbon and later revisited and confirmed in several subsequent works [1, 18-22].

Hysteresis and scanning phenomena require a model that goes beyond a single, slit shaped pore. Two alternative classes of activated carbon models have been proposed that are not based on the slit pore presentation. In the first class, construction of the model of a porous microstructure aims either to reflect the actual process of activated carbon formation or capture essential structural characteristics such as the radial distribution function between carbon atoms (see for example, Ref. [23]). This type of reconstructive methods typically lead to complex, disordered models of carbon microstructure. In the second class of models a similar overall effect of structural disorder and heterogeneity is achieved by considering a system of randomly packed structural elements, representing reasonably realistic fragments of stacked graphite layers [24-27]. These non-slit pore models of activated carbons so far have been used predominantly to provide a qualitative explanation for the observed adsorption phenomena and only recently attempts to extend them to quantitative adsorption predictions have been made [8, 9].

In the context of water adsorption, these non-slit pore models confirm the original picture proposed by Gubbins and co-workers. For example, Liu and Monson explored a model of BPL activated carbon based on a random packing of carbon platelets, or disks, decorated with polar surface groups [26]. Again, adsorption of water starts at these groups, followed by formation of clusters of various sizes in different compartments of the model. Interestingly, this model is able to reproduce very realistic adsorption isotherms, including the hysteresis

loop. Although water scanning curves have not been explored in this model (or for that matter in any other model), realistic hysteresis loops observed by Liu and Monson suggest that this class of models is a promising starting point to explore scanning adsorption behaviour.

Hence, our starting point is the model of a high surface activated carbon based on a random packing of curved, fullerene-like fragments of carbon sheet decorated with polar surface groups [8, 9]. Previously, this kind of model has been used to investigate carbon dioxide and methane adsorption in Maxsorb activated carbon (or MSC-30) and adsorption of multicomponent mixtures, relevant for carbon capture processes [8, 9]. A similar model has been also recently employed by Wang *et al.* with a focus on the role of surface groups on carbon dioxide/methane separation factors [28]. In the historical perspective, this model indeed stems directly from the studies of Liu and Monson [26] and Segarra and Gland [24] before them, based on simplified or coarse-grained models of graphitic fragments. However, explicit representation of the molecular structure of the fragments provides a more flexible way to control and explore various properties of the fragments such as geometry, location and type of the surface groups. It also makes it possible to use reasonably accurate off-the-shelf force fields without excessive re-parameterization and explicitly include charge distribution within the fragment. Several other similar fragment-based models have been proposed recently [29-31], however water adsorption, including hysteresis and scanning phenomena, have not been explored in them, most likely due to prohibitive computational cost, as will be discussed later in the article.

The remaining article is organized as follows. After the methodology section, we first present experimental data for water adsorption in MSC-30 at 308K and place our findings in the context of the previous experimental studies on similar materials. We will then compare the experimental results with simulations. The model proved to be computationally very

costly (we will touch upon this issue in the Conclusion section) and, as a result, comprehensive optimization of the model to reproduce experimental results could not be performed at this stage. Therefore, the comparison between the model and experimental data is still qualitative (or rather semi-quantitative as we present results in reduced units of pressure, and in experimental units of loading and the simulation isotherms operate in the correct ranges of those variables). Using the results from molecular simulations we investigate properties of the water clusters along adsorption and scanning isotherms. Molecular visualization provide additional insights on the state of the system along these paths.

2. Methodology

2.1 Experiments: characterization and water adsorption

The porous material used in this study has already been used and characterized in our previous work [8]. The BET surface area and the pore volume measured for the Maxsorb MSC-30 are respectively 3179m^2/g and 1.33cm^3/g. The characterization and activation of the sample have been performed on a Quantachrome Autosorb IQ apparatus coupled with the Quantachrome ASiQwin software for the automated acquisition and reduction of the data. The pore size distribution (see the SI) and the micropore volume have been calculated QSDFT method [32].

The experimental equilibrium isotherms have been measured on a Quantachrome Aquadyne DVS gravimetric water sorption analyser. The instrument is a gravimetric system which operates at atmospheric pressure and constant temperature under different partial pressure of water vapour. Both the temperature and the relative humidity of the gas phase in the sample chamber are continuously monitored respectively by a Pt-100 thermocouple and a

humidity probe with an accuracy of ±0.8 RH. A proportional-integral-derivative (PID) controller continuously mixes a humid stream and a dry nitrogen stream. The total flowrate entering the sample chamber is about 50 cm^3min^{-1} and for obvious reasons the flow does not directly hit the sample in the crucible. The system has been calibrated and the PID parameters set to give a step-wise concentration change in the gas phase. The correction for the buoyancy of the sample is negligible considering low density of the gas phase. All the experiments have been performed using the same sample which had previously been activated for 4h at 150^oC under vacuum. An entire adsorption/desorption isotherm, two desorption and two adsorption scanning curves have been measured. The equilibration time has been independently chosen for each point in order reach equilibrium at a given relative humidity P/P_0. Some of the experimental points have shown quite a long equilibration time up to 30 hours.

2.2 Molecular simulations

The molecular model of Maxsorb MSC-30 follows the strategy developed in our previous publications [8, 9]. It is based on a random packing of fullerene-like structural elements, functionalized with polar surface groups. In the previous publication, we concentrated on a model where a single corannulene molecule was functionalized with two hydroxyl groups. The model was calibrated and validated in application to carbon dioxide and methane adsorption at ambient temperature conditions; in application to adsorption of water at 298K, the model produced an S-shaped isotherm, qualitatively similar to the experimental data, but shifted to higher relative pressures, thus indicating a more hydrophobic character of the surface compared to the actual material [9]. To alleviate this problem, here we consider a variant of the model where each corannulene is functionalized with three carboxyl groups, known to have stronger interaction with water. We emphasize here that the objective of the study was not to achieve a perfect quantitative agreement with the experimental data, but

have a reasonable qualitative agreement in the range of pressures comparable the experiments.

Figure 1, on the left, shows molecular visualizations of the structural element from two different perspectives; as can be seen from these visualizations, having the 5-member ring in the centre of the corannulene molecule makes it curved. The geometry of a single structural element is optimized using quantum-mechanical methods (see details below) and then in the all the consecutive processes is treated as rigid. On the right, Figure 1 shows the final structure obtained after random packing of 190 structural elements in a cubic cell with a side length of 60Å. The model was developed to reproduce key structural characteristics of MSC-30 and comparison between the properties of the model and the prototype material is provided in Table 1. From Table 1 it is possible to see that the features of the model quite closely follow the features of the target material. In the SI, the geometric pore size distribution is also compared to the original results from Otowa *et al*. [33], NLDFT and QSDFT analysis [32, 34]. These results can be summarized as follows. In the molecular model, generally, most of the groups are centred around 5Å pore radius. This region of the PSD is an excellent agreement with the predictions from the accurate QSDFT approach [32]. The real sample also contains a range of pores centred around 9Å in radius (according to QSDFT) and extending up to almost 25Å in radius. The pore volume analysis based on QSDFT estimates the total pore volume at 1.53 cm^3/g, while pores of up to 10Å in radius (micropores) are responsible for 1.12 cm^3/g (73%) of this pore volume. The micropore volume is also in a good agreement with the pore volume of the molecular model (1.215 cm^3/g). We further note that the current approach is not concerned with the mechanical stability of the model structures.

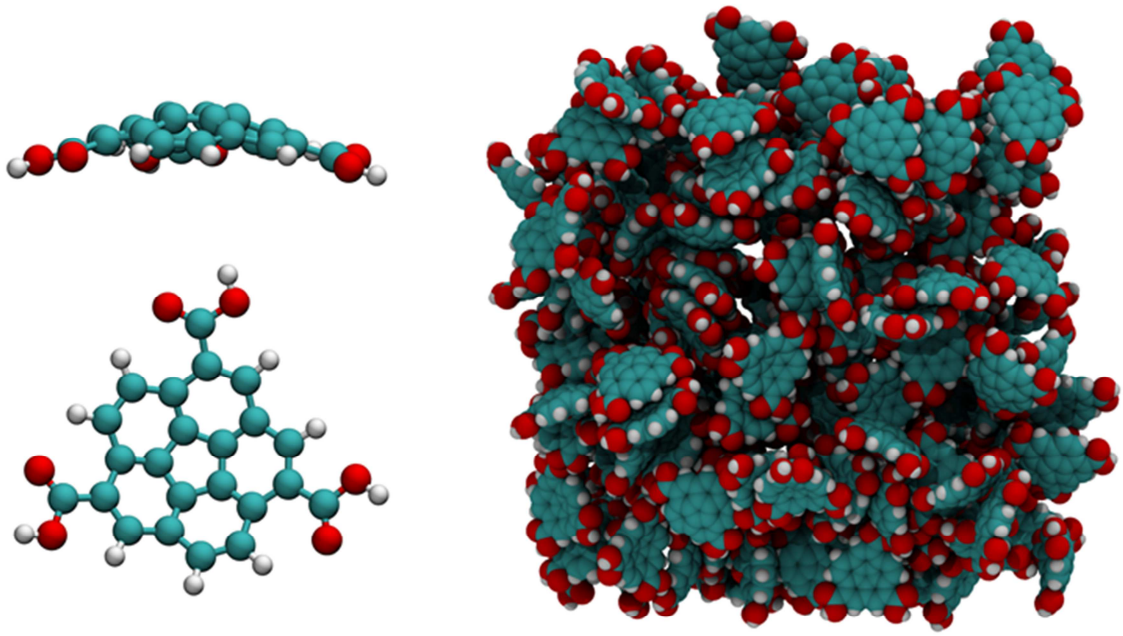

Figure 1. Computer visualizations of a corannulene-like element functionalized with three carboxylic groups from two different perspectives in the cpk representation (on the left). The final structure (190 elements in a cubic cell of 60 Å in size) obtained from random packing of the individual elements (on the right). Cyan: carbon, red: oxygen, white: hydrogen.

Table 1. Characteristics of the model structure based on a packing of corannulene-like elements functionalized with three carboxyl groups (Model), compared to the experimentally measured typical properties of Maxsorb MSC-30 (MSC-30). In this table, S.A. is the surface area, V is the micropore volume and C/O is the carbon/oxygen ratio (in weight) in the material. We use QSDFT [32] to obtain the pore volume of the experimental sample, with the volume of pores of up to 10Å in radius shown in brackets.

SYSTEM	**S.A.** $\mathbf{m^2/g}$	**V,** $\mathbf{cm^3/g}$	**C/O**
Model	3337	1.215	2.8

MSC-30	3179	1.530 (1.120)	7.8

Surface area and micropore volume (from computational Helium porosimetry) of the packing of structural elements have been calculated using Poreblazer 3.0.2, a package of simulation tools developed by Sarkisov and Harrison [35]. These structural characterization tools are also employed to calculate pore size distribution, surface area, pore limiting diameter and other characteristics of the systems, containing water at a specific point on the adsorption isotherm. Further details on the construction and characterization of the model can be found in our previous publications [8, 9].

For all our adsorption simulations we use the energy biased grand canonical Monte Carlo method (GCMC), as implemented in the MuSiC simulation package [36]. Adsorption and scanning branches of the isotherm are generating by progressively increasing or decreasing the water vapour pressure, respectively, starting from the previous configuration on the isotherm. Desorption scanning curve is obtained by reversing the adsorption process at P/P_0 before the closure of the hysteresis loop. All adsorption data is reported as absolute amount adsorbed (mmol/g). Further details of the GCMC simulation protocol adopted in this work, including details of the potential cut-offs, type and weight of Monte Carlo moves and other parameters, are provided in the SI file, however here it is important to emphasize that equilibration of the adsorbed states along the adsorption isotherm and within the hysteresis loop is an extremely slow process and requires between $3 \cdot 10^8$ to $1.5 \cdot 10^9$ Monte Carlo trials per point, although several studies have explored and argue for even longer runs based on the number of successful Monte Carlo moves per molecule [37-39]. We acknowledge here that whether an adsorption point for water in an activated carbon is truly equilibrated remains a challenging issue for both simulations and experiments.

For molecular dynamics (MD) simulations we employ Gromacs simulation package (v5.1.2) [40]. Each simulation runs for 5 ns, with 1 fs time step. Constant temperature is maintained via the Nose-Hoover thermostat. Other parameters of the MD simulations are summarized in the SI file.

The full set of Lennard-Jones (LJ) parameters associated with the model structure for the adsorbent is reported in the SI. The LJ parameters mostly correspond to the ones proposed by Tenney and Lastoskie [41], which are also in line with other parameters reported in literature. Partial charges are calculated using the B3LYP Density Functional Theory method [42], with 6-31G basis set and CHELPG [43] charge analysis using the Gaussian 09 software package [44]. This is also the method used to obtain the energy minimized geometry of the corannulene molecule, modified with three carboxylate groups. For water we adopt the TIP4P model [45] also used in our previous publication [8, 9]. The NIST database for standard reference simulation properties is employed here to estimate the TIP4P vapour pressure at 308K (10.0 kPa)[1]. In the SI file, we also provide additional details on the energetics and structural features of a complex between a single water molecule and the carboxylate group.

Analysis of the water clusters is performed according to the following methodology. A water molecule is considered to be a part of a cluster if it is associated either with a surface group or another water molecule. We consider clusters that contain at least two water molecules. Two water molecules are considered to be connected if the distance between their oxygen atoms is less than 3.5Å (this distance corresponds to the first minimum in oxygen-oxygen radial distribution function for the bulk liquid water at ambient conditions). A pathway, consisting of these pairwise connections can be constructed for any two water molecules within a cluster. A simple recursive algorithm is used to calculate the distribution

[1] The NIST Chemistry WebBook, http://webbook.nist.gov/

of the clusters in the system given the xyz coordinates of the oxygen atoms and the mean cluster size M_{cl} using [46]:

$$M_{cl} = \frac{\sum_k k^2 n(k)}{\sum_k k n(k)} \qquad (1)$$

where k denotes cluster size (number of particles in the cluster) and $n(k)$ the number of clusters of size k.

Isosteric heat of adsorption is calculated using a well-known expression based on the energy and number of molecules fluctuations in the grand canonical ensemble:

$$q_{st} = RT - \frac{\langle UN\rangle - \langle U\rangle\langle N\rangle}{\langle N^2\rangle - \langle N\rangle^2} \qquad (2)$$

where properties in brackets are ensemble averages based either on number of molecules N or energy of interaction U, R and T are the gas constant and temperature as usual.

Other details are introduced in the Results section as needed or summarized in the SI file.

3. Results

We begin this section by focusing on the experimental results. Adsorption isotherms for water in the MSC-30 sample at 308K are shown in Figure 2. As expected the isotherm shows Type V behaviour typical for many activated carbons. Whether the hysteresis loop should be qualified as H1 (typically associated with independent pore domains) or H2 (typically associated with the network effects) is rather subjective. In the panel on the left we also provide comparison of the results for MSC-30 with that for SAC31 at 303K, which shows a

hysteresis loop somewhat closer to H2 type [47]. SAC31 is also variant of Maxsorb material, obtained via KOH-activation of a coal-based carbon, but with slightly different structural characteristics compared to MSC-30: lower surface area (2290 m^2/g), lower volume (1.33 cm^3/g), lower oxygen content (C/O 9.1) [47]. Comparison of nitrogen sorption isotherms at 77K for two materials is provided in the SI.

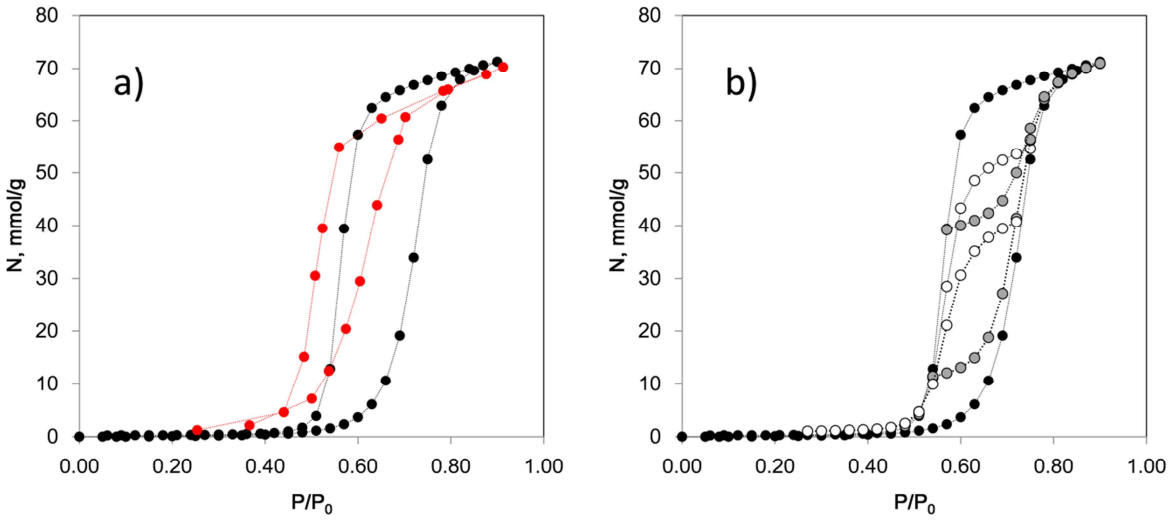

Figure 2. a) Adsorption isotherm for water in MSC-30 at 308K (black symbols, this work) and in SAC31 at 303K (red symbols, Miyawaki *et al.* [47]). b) Adsorption isotherm for water in MSC-30 at 308K shown together with two adsorption scanning curves (grey symbols) and two desorption scanning curves (white symbols). In all graphs lines are for eye guidance only.

Scanning behaviour (using two adsorption and two desorption processes) is shown on the right panel of Figure 2. One notices that the scanning curves mimic the shape of the boundary adsorption and desorption isotherms, first crossing the hysteresis loop and then closely following the sharp changes in the adsorbed densities.

In Figure 3, we compare side by side (qualitatively) experimental adsorption behaviour (panel a) and predictions from the molecular model (panel b). Here we focus only on the adsorption branch and one scanning desorption curve. The desorption branch of the isotherm

is not considered here as the Monte-Carlo simulations tend to exaggerate the extent of the metastable desorption branch of the isotherm leading to unrealistically large hysteresis loops and discontinuous transition from high adsorbed amount to low adsorbed amount on the desorption branch (so the scanning adsorption behaviour cannot be investigated using this desorption isotherm, as it provides no starting points for the process). The reason for this is that in molecular simulations, a relatively small sample of a porous material is considered in periodic boundary conditions. Upon desorption and according to the adopted protocol, the system starts from a point where the porous material is completely filled with the dense adsorbate. Within this model, however, there is no direct interface between the structure and the bulk phase and hence there is no mechanism to initiate the desorption process, leading to the system running into highly improbable metastable regions. In principle, this can be addressed by either considering a model where the porous material region is placed in a direct contact with bulk regions or where some other means of introducing the initial nucleus of the confined vapour phase are used. It is possible that more advanced simulation setups with explicit control volumes will allow us to circumvent this problem in the future and produce a more complete picture; however it has not been pursued in this article due to substantial computational cost.

Before we consider molecular organization of the confined water in the model structure, it is important to highlight the key differences between the experimental results and the simulations. Below we enumerate these differences and provide the plausible reason for them. As we will see these differences stem predominantly from model being a purely microporous structure whereas the actual material features both micropores and mesopores (see structural analysis data in the SI). The differences are highlighted as we progress from lower to higher pressures:

a. The slope of the adsorption isotherm in the pressure range $P/P_0 < 0.4$

The experimental isotherm has almost no adsorption up to start of the hysteresis loop whereas the model predicts some adsorption in this range. This in fact presents some challenge for the construction of the molecular models. On one hand, smooth variation of the adsorbed density on the adsorption isotherm in the hysteresis region does require presence of a sufficient number of surface groups in the model[9]. However, at the same time, having many surface groups also makes the material apparently more hydrophilic compared to the experimental sample. This poses an important question on how the actual surface groups are organized in the real material so that the behaviour is captured correctly.

b. Location of the hysteresis loop on the pressure scale.

Location of the adsorption isotherm (even in reduced units) is sensitive to several features of the model such as presence and concentration of surface groups, and it is highly unlikely to capture the correct position without some additional optimization involved.

c. *Total amount adsorbed and shape of the isotherm after the closure of the hysteresis loop.*

As can be seen in the experiments, the adsorbed amount continues to increase after the closure of the hysteresis loop, whereas in the molecular model a very definite saturation is reached, leading to a well-defined plateau in the adsorbed amount. This is a result of presence of some mesopores in the actual sample, where water should not condense in the pressure range shown, but it continues to adsorb in these pores, as well as on the surfaces of the sample. In a purely microporous model, in the absence of mesopores or explicit interfaces with bulk, this is not the case. The difference between the total porosity of the sample and porosity of the model is also responsible for the differences in the amount adsorbed at higher pressures.

d. The lower pressure portion of the scanning curve is smoother and features more points compared to a step change in the simulations.

We will return to this issue in the Conclusions sections once we develop a picture of what happens along the scanning curve in the model.

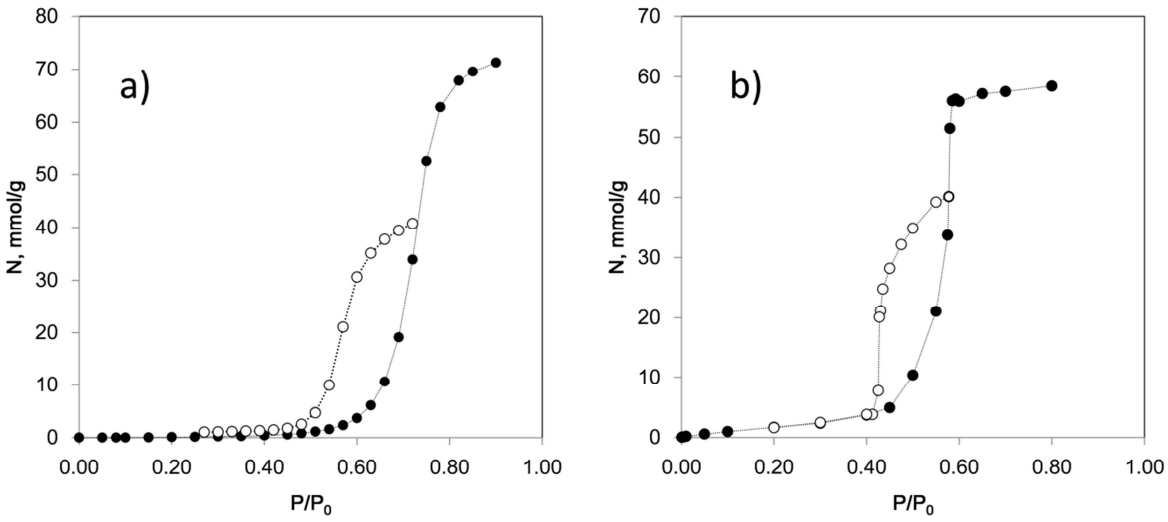

Figure 3. a) Experimental isotherm for water in MSC-30 at 308K (adsorption branch only, black symbols) shown together with a single desorption scanning curve (white symbols). b) Simulated adsorption isotherm for water in MSC-30 at 308K, following the same notation for the symbols as panel a). In all graphs lines are for eye guidance only.

7

In Figure 4 we show a series of snapshots corresponding to different states of the system along the adsorption and scanning curves.

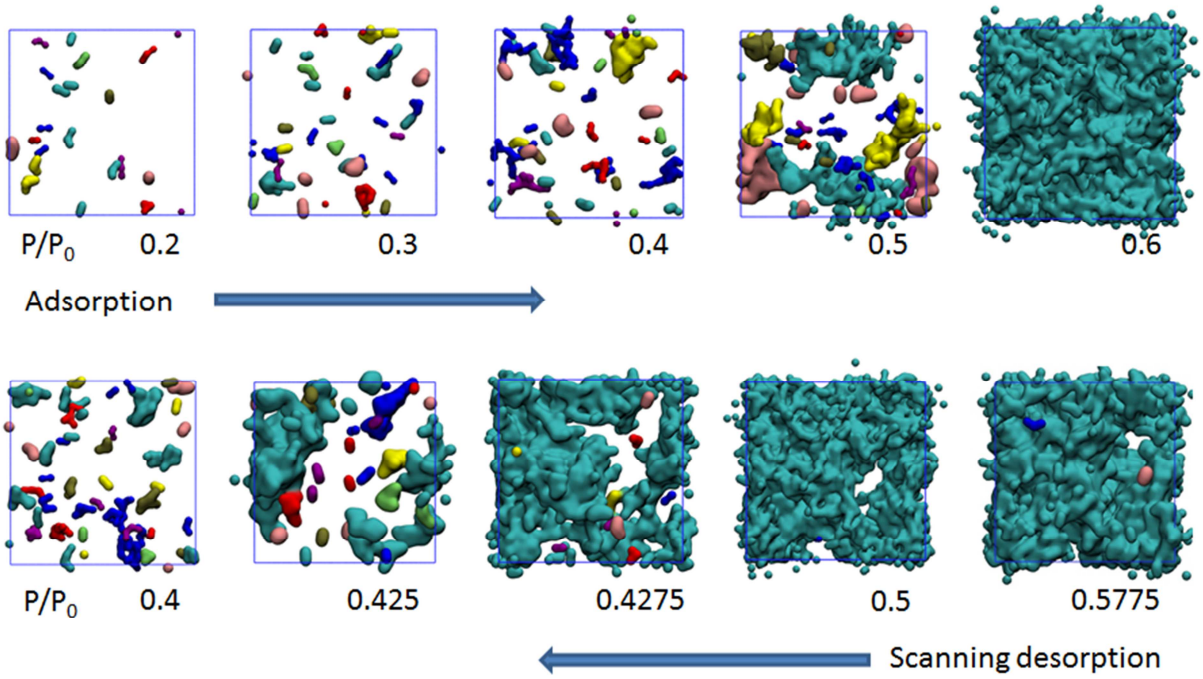

Figure 4. Molecular visualizations of the water clusters during different stages of adsorption process (upper panel) and scanning desorption process (lower panel), in the accessible surface representation. Each visualization corresponds to a particular value of the relative pressure indicated under the snapshots. Colouring is used to distinguish separate clusters, however the actual colours do not have any specific meaning. Note, that although some clusters appear as disjoint, they may be connected over the periodic boundaries.

Let us first focus on the adsorption process. Clusters start forming at about P/P_0=0.1 (not shown). Below this pressure water exists as individual water molecules bound to the surface groups. As the pressure increases, the clusters grow in size, and also new clusters form in less favourable locations (see further analysis below). Around the P/P_0=0.4 clusters begin to coalesce and in the intermediate pressures around P/P_0=0.5-0.55 the system features large disjoint clusters, which progressively bridge until a single cluster is formed. In the final stages of the process (P/P_0=0.6) the system fills the remaining voids, with apparently unfavourable interaction with water (hydrophobic cavities of about 7-8Å in diameter,

according to the structural characterization of adsorbed states). This is also the regime that in our case provides the starting configuration for the desorption scanning curve. It starts from a system, featuring one percolating water cluster (in other words the cluster spans across periodic boundary conditions in all three dimensions) and a large bubble of about 7-8Å in diameter, providing the initial vapour-liquid interface. At the beginning, the system goes through a series of states where the bubble increases in size and new empty regions form, while the water molecules still remain a part of one large percolated cluster. In essence it is a process of water evaporation from the surface of a single cluster and vapour-liquid interface receding as the desorption progresses. The cluster disintegrates into smaller sub-clusters around P/P_0=0.425 and finally at about P/P_0=0.4 the system returns to a state of a large number of disjoint small water clusters. We note here that comparing to the experimental scanning curves, this stage of the process is less smooth in simulations and the transition into smaller clusters is rather abrupt. One possible explanation for this is a limited size of the system under consideration. However, as we will further discuss in the Conclusions section, increasing the system size is likely to be computationally prohibitive for the current molecular simulation approaches.

An alternative way to summarize these processes on adsorption and scanning curves is by using a diagram where x-axis corresponds to the size of the water cluster, grouped in brackets of up to 10 molecules, 10-100, 100-500, and 500-5000 molecules in the cluster, y-axis corresponds to the number of clusters of certain size. A point on this diagram would tell us the number of clusters (y) with size in a specific bracket. Furthermore, we use the size of the circle placed at a particular x-y location to indicate fraction of water molecules that is contained in the clusters of a certain range. A system with a large number of small clusters would have a circle (or circles) located in the top left corner of the diagram; a system corresponding to completely filled pores (one percolated cluster) will sit at the far right side

of the x-axis and y=1. Indeed, these diagrams, corresponding to the same states of the system as in Figure 4, are summarized in Figure 5.

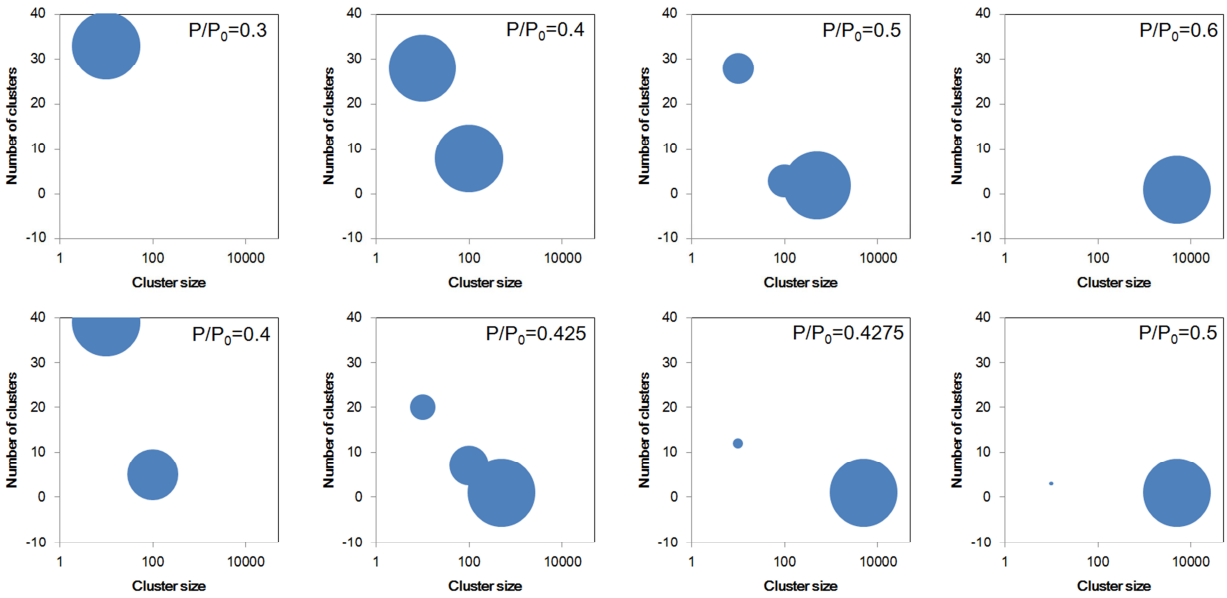

Figure 5. Cluster population diagrams for adsorption (top) and desorption scanning (bottom) states. Here, x-axis is the size of the cluster in ranges of <10, 10-100, 100-500, 500-5000 molecules in the cluster, y-axis is the number of clusters with the size up to x molecules, size of the circle corresponds to the fraction of molecules contained within the clusters of a certain range.

Additional analysis is provided using several alternative metrics associated with the clusters. In particular, we focus on the number of clusters and average cluster size, Figure 6. We note here that both properties are calculated for the final configuration of the simulation run at a particular pressure point and are not averaged over multiple system configurations. As a result they do show some degree of scattering, however the general trends are quite visible and this will suffice for the analysis here. Up to pressure of P/P_0=0.4 the average cluster size remains small and changes very little, while the number of clusters increases. P/P_0=0.4 corresponds to a sharp peak in the number of clusters after which it quickly

diminishes indicating the coalescence process. Naturally, the average cluster size rapidly increases in this region. The same characteristics can be plotted for the scanning curve, confirming that the P/P_0=0.4 is the boundary between the system in a state with multiple disjoint clusters and the system in a state where clusters start to coalesce.

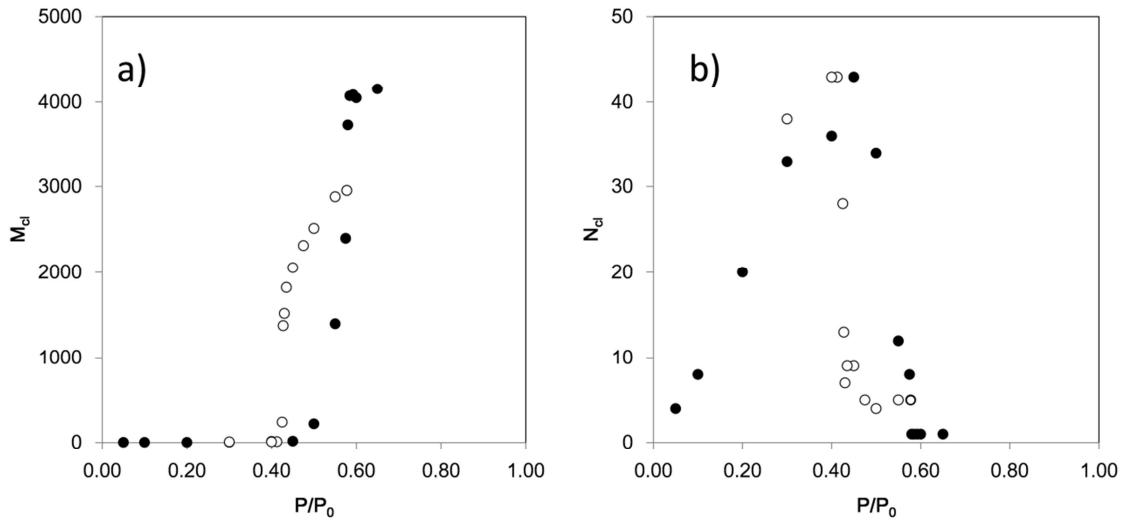

Figure 6. a) Average cluster size M_{cl} as a function of reduced pressure P/P_0. b) Number of water clusters in the system as a function of relative pressure P/P_0. In both graphs, filled circle correspond to the adsorption isotherm (not extended beyond P/P_0 =0.65 as the property become essentially constant), while open symbols correspond to the scanning desorption curve.

In summary, we observe that different key boundary points of the hysteresis loop are associated with different distinct states of the system. The inception of the hysteresis loop is linked to the process of water clusters coalescing with each other. The hysteresis loop is closed when the system is completely filled with water. The desorption scanning behaviour samples a different pathway, where the density of the system recedes by gradual evaporation of water from the surface of connected single cluster, which is different from the process of large clusters bridging with each other during the adsorption.

We now would like focus on the comparison of the states of the system at P/P_0=0.5 on the adsorption and P/P_0=0.425 on the scanning curve. These states are of different but comparable density. However as seen from the molecular visualizations, these states correspond to completely different arrangement of water clusters, in terms of their size and location (Figure 4). Molecular dynamics simulations in NVT ensemble (see the SI video) of the system corresponding to P/P_0=0.425 on the scanning curve show water clusters confined and fluctuating in their cages (or cavities) and bringing the system to 500K changes only the vigorousness of the fluctuation but not the structure and the arrangement of the clusters (see SI videos). We have not investigated dynamic properties of the system, such as self-diffusion coefficient, as it requires much longer simulation times to obtain reliable data (hundreds of nanoseconds, according to Farmahini *et al* [48]). To further investigate stability of the system on the scanning curve at P/P_0=0.425 we perform the following study. The system is first brought to 1000K within the canonical ensemble Monte Carlo simulation. The resulting system, featuring no large clusters, is returned back to 308K and considered either at the same relative pressure (P/P_0=0.425) or at a constant density within the canonical ensemble. As we show in the SI file, in the first case the system ends up in a state of lower density with the structure very similar to the neighbouring pressure state on the adsorption curve. In the second case, the system shows an arrangement of clusters that is different from the starting configuration on the scanning curve, however it is not clear whether this state corresponds to a state on the adsorption curve or it is a different metastable configuration altogether.

The analysis above provides a molecular-level picture of the structural differences between the states of the system on the desorption scanning curve and on the adsorption isotherm at relatively low adsorbed densities, where confined states feature separate clusters. What about the first several points on the scanning desorption curve, where it starts from the adsorption isotherm, but as we decrease pressure follows a different pathway of the adsorbed states with

higher density, compared to the adsorption isotherm? As we have already discussed, in this range of densities (>20 mmol/g) states on both the adsorption isotherm and the scanning curve correspond to a single percolated water cluster. Structural analysis (using the Poreblazer software) shows that the states of comparable density on these branches have very similar structural characteristics, such surface area of the percolated water cluster, pore limiting diameter and the size of the largest cavity in the confined water phase. Yet, the shape of these clusters is different (not shown). This implies, that although the receding liquid-like phase remains connected and forms a single cluster for a range of decreasing pressures during desorption scanning, it apparently follows a different set of states from the process where this phase is gradually growing along the adsorption branch.

Thus, within hysteresis loop we can identify alternative states of different loading and structure corresponding to the same relative pressure, or states of the same adsorbed density but corresponding to the different relative pressure values and featuring different spatial organization of the adsorbed phase. Recently, it has been suggested that even a single point within the hysteresis loop corresponding to a specific loading and relative pressure, may in fact be a proxy for several alternative states of the system, depending on the pathway by which this point has been reached [49].

We now turn our attention to the interaction energy aspects of the adsorption and scanning processes. An interesting question is how clusters interact (and if they interact) with each other prior to coalescing. In Figure 7 we consider different components of the total interaction energy for a particular state at P/P_0 =0.4, which corresponds to the peak in the number of clusters as well as opening of the hysteresis loop (a complete picture for other pressure points is provided in the SI). From this figure it is clear that the interaction between water molecules and the solid structure and among water molecules is dominated by the Coulombic interactions. In fact, these interactions may force the molecules to be very close to

each other, leading to the unfavourable dispersion contribution (the Lennard-Jones component). Interestingly, according to Figure 7, the long range Coulombic interactions are essentially zero between the individual water clusters, which can be explained on the grounds of the clusters being electrostatically neutral. Water clusters may also have a net dipole moment due to a particular juxtaposition of water molecules [50] and it would be also interesting to explore their dipole and higher order moments as a function of size, structure and confinement. The Lennard-Jones interactions between the clusters are weak as most of them are located at distances >15Å between their constituent molecules; however as the density increases we see a small favourable LJ term present in the cluster-cluster interactions.

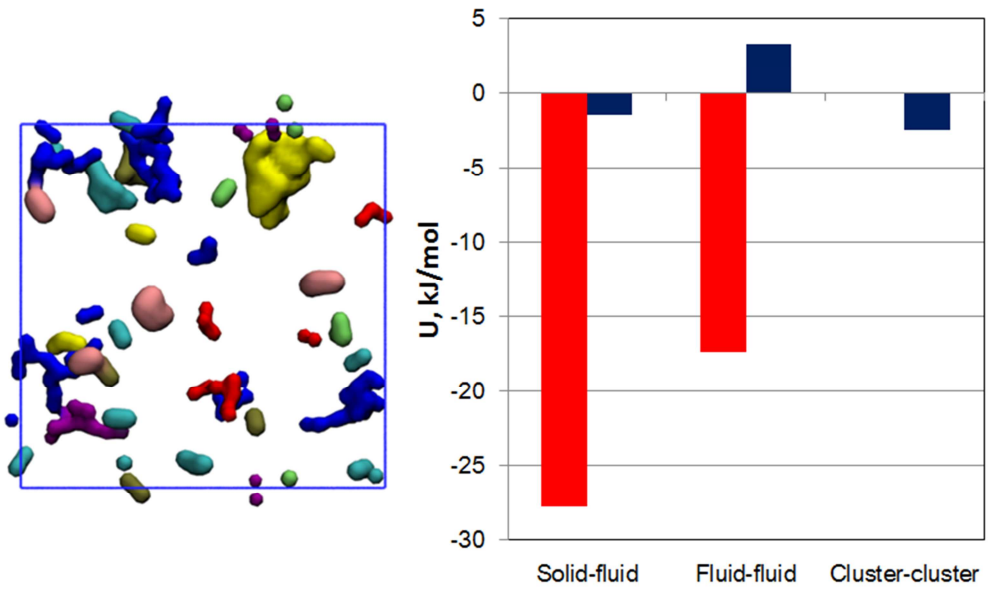

Figure 7. Different contributions to the total interaction energy at P/P_0 =0.4 (3.7 mmol/g) on the adsorption isotherm (on the right). Red corresponds to the Coulombic interaction energy, dark blue corresponds to the Lennard-Jones interaction energy. Here fluid-fluid interactions correspond to the interaction between the molecules within a cluster and interactions between molecules of different clusters. The molecular configuration of the clusters under consideration is shown on the left (adsorbent structure is not shown for clarity).

Figure 8 (a) plots isosteric heat of adsorption for selected pressure points on adsorption and scanning curves. Although there is some degree of scattering, it is possible to deduce the overall trend: at very low loading (<0.1 mmol/g), water molecules interact with particularly favourable sites, likely involving more than one surface group and leading to the values of the isosteric heat of adsorption 50-60 kJ/mol; at higher loading isosteric heat converges to the expected bulk water heat of evaporation value (here about 45 kJ/mol). Although this trend is similar to that reported in earlier experiments (see, for example, studies on BPL carbon[51]), we find it difficult to reconcile these results with the experimental behaviour of the MSC-30 sample in this study, which shows very little adsorption at lower pressures almost up to the opening of the hysteresis loop We also note a spike in the isosteric heat at loadings of 30-50 mmol/g. On the adsorption isotherm this corresponds to a narrow pressure range of P/P_0=0.575-0.58, where the single percolating cluster of water has already formed and the final change in density is associated with the closure of the remaining cavity. Whether it is a spurious result, due to poor sampling, a specific property of the current model, or a more general effect is yet to be established, however we note that a similar result has been observed on hydrophobic carbons by Nguyen and Bhatia [52].

Interaction between water molecules and surface groups plays the key role in our interpretation of water adsorption isotherms and in construction of theoretical and phenomenological models of water adsorption. The picture typically drawn involves several distinct stages: water molecules first associate with the surface groups and form nuclei of the clusters; then the clusters grow and coalesce (see for example, Ref. [53] among several studies building on this picture). Here, within the developed molecular model, we can directly explore how many groups are occupied by water molecules as adsorption progresses. For this we need to define the state of the surface group occupied by a water molecule, as several alternative definitions are possible. Naively, we may propose that a surface group forming a

hydrogen bond with a water molecule should be declared as occupied. However, the carboxyl group can form two hydrogen bonds. Furthermore, several definitions of the hydrogen bond exists and it is plausible that the carboxyl group forms more than two associations with water molecules, with the energy and geometry of these associations deviating from the strict definition of the hydrogen bond (if we wish to adopt one). Alternatively, a single water molecule can be engaged with more than one surface group, depending on a particular spatial arrangement of these groups. Here, we use a simplified approach. We postulate that a surface group is associated with a water molecule if there is a water molecule in its vicinity and the distance between the oxygen atom of the water molecule and any of the oxygen atoms of the carboxyl group is less than 3Å (according to the quantum mechanical-calculations, if a hydrogen bond is formed, this distance should be 2.8Å). Therefore, a group associated with more than one water molecule is counted as occupied only once; on the other hand if a water molecule forms an association with more than one group, all these groups are counted as occupied. In Figure 8 (b) we plot the fraction of surface groups, occupied according to our definition by a water molecule, as a function of pressure. As can be seen from this figure, we do not observe any plateau which would indicate saturation of the accessible surface groups with water molecules; in fact the fraction of surface groups associated with water molecule continue to grow along the adsorption branch until the closure of the hysteresis loop reaching the saturation value of about 84%. Thus, in the sparse structure of the proposed model a substantial number of surface groups (about 84%) is geometrically accessible with respect to water molecules (according to our definition), however not all of them necessarily offer energetically favourable interactions, due to geometrical constraints. On the other hand, close proximity of two or more surface groups may offer a particularly favourable interaction site, and the existence of these sites is supported by the data on the heat of adsorption. At a low pressure the most favourable binding sites and surface groups are occupied first, however as

adsorption progresses all of the porous space eventually becomes occupied with water and interactions are formed between water molecules and less attractive surface groups. This draws a picture of a substantial heterogeneity of the quality and energetics of the surface groups, depending on their location. Although this may be a particular feature of the model we use, such heterogeneity of binding sites will have important implications for the proposed approaches to use water to probe concentration and type of surface groups.

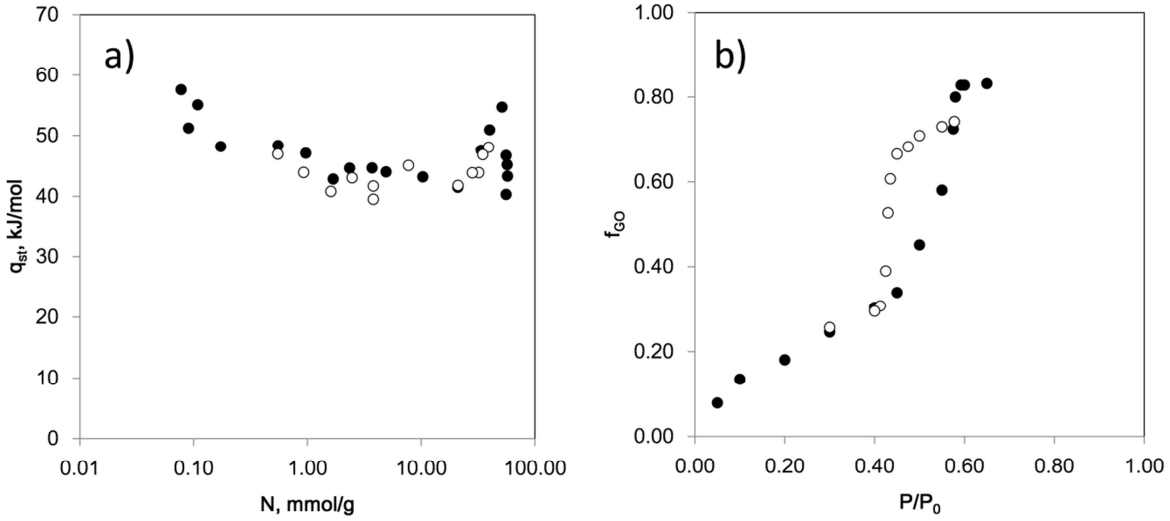

Figure 8. a) Isosteric heat of adsorption, q_{st}, as a function of loading (mmol/g). b) Fraction of water-occupied surface groups (see definition in the text) as a function of relative pressure P/P_0. In both graphs, filled circle correspond to the adsorption isotherm (not extended beyond P/P_0 =0.65 as the property become essentially constant), while open symbols correspond the scanning desorption curve.

4. Conclusions

This study can be summarized as follows. Using experimental data on the structure of the high surface area activated carbon, Maxsorb MSC-30, we constructed a molecular model of this material that reflects some of its characteristics: specifically, disorder, high surface area and porosity, and complex distribution of surface groups. This model, in application to water

sorption, qualitatively captures some features of adsorption and scanning desorption curves. From this perspective, it can be considered as a good starting point to develop more quantitative models.

The adsorption branch within the hysteresis loop corresponds to a two-phase process: 1) water clusters coalescing with each other; 2) followed by formation of a single percolated water cluster, which then grows until the system is filled, and at this point hysteresis loop closes. We show that the desorption scanning curve is predominantly associated a single water cluster shrinking in size via evaporation, followed by the disintegration in a series of smaller clusters. Schematically, this picture is summarized in Figure 9. We note that in other carbon materials and models the nature of the hysteresis and scanning could be of a different nature [48] and the universality of these observations is yet to be tested.

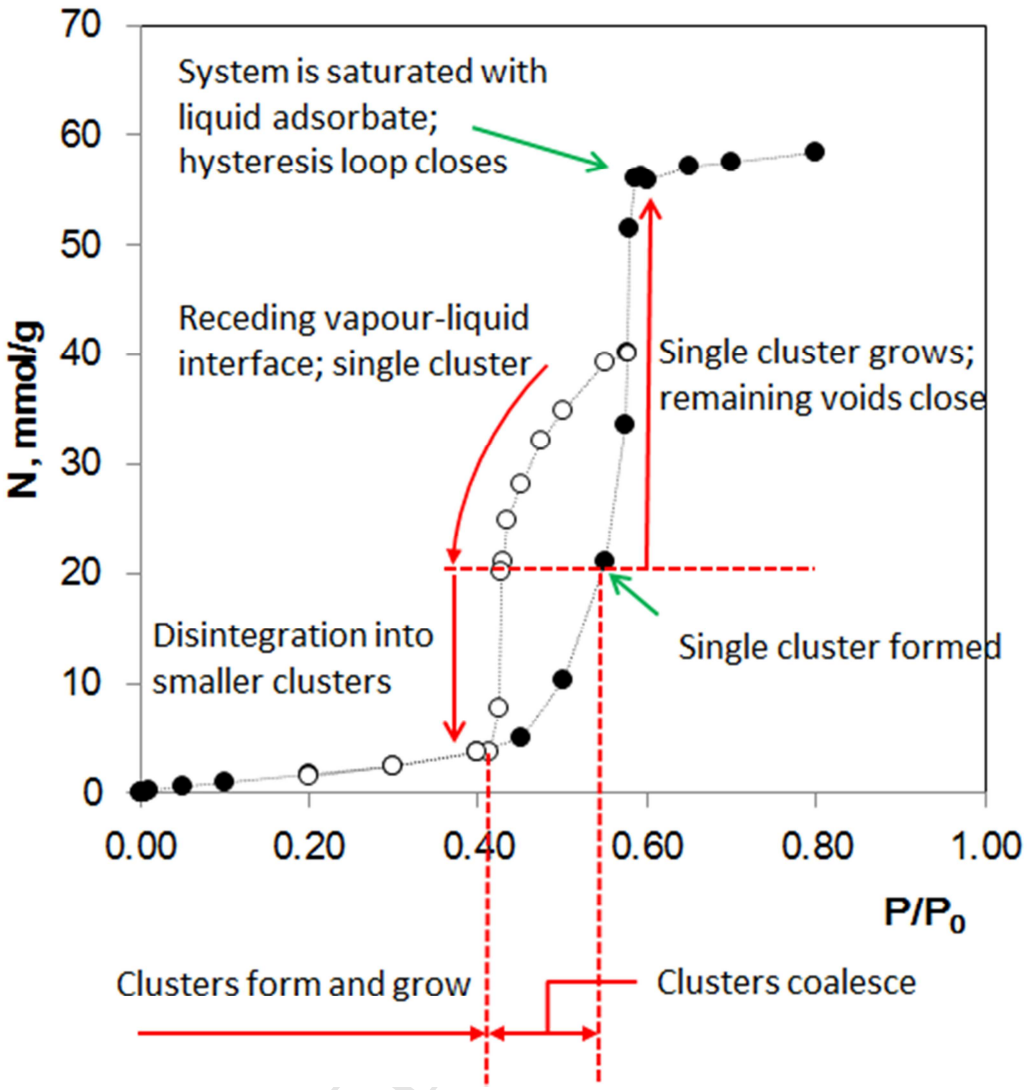

Figure 9. Schematic depiction of the regimes observed for adsorption and scanning desorption curves.

The picture of activated carbon where the water adsorption process is initially driven by the surface groups and once they are occupied the remaining less favourable regions fill with water is not quite correct. In fact, during the density increase more interactions form between water and surface groups, but these interactions are simply not as favourable as the ones governing the early stage of the process.

We now return to the issue of the steep step on the scanning curve associated with the disintegration of the system into small clusters and lack of this step on the smooth

experimental scanning curve. Two possible hypotheses can be offered for to explain this difference. One possibility is that it is associated with the limited size of the model and hence lack of additional intermediate metastable states on the scanning curve. Another possibility is that in the real material the stage associated with a single percolated cluster receding through the evaporation from the interface is prolonged to lower pressures compared to the model. Both of these hypotheses require further investigation.

It is now evident, on a hindsight, that the proposed model is a model of a high surface activated carbon with a relatively high concentration of surface group, but it is not quite a model of MSC-30. However, it provides an important starting point for further developments. Of course a single desorption scanning curve is not enough to build a comprehensive theory of water scanning behaviour in activated carbons and how it is governed by their structure and surface properties. For this, the current analysis must be extended to more scanning curves from different starting positions, to adsorption scanning curves and to other materials and temperatures. Furthermore, it will be important to explore other models of water with more accurate thermodynamic behaviour under conditions of interests, such as for example more recent and advanced variants of TIP4P [54].

Another important feature of MSC-30 (and many other activated carbons) is presence of mesoporosity. Unfortunately, it is not easy to include mesopores in the molecular model. One way would be to introduce a slit-like gap in the system, as has been done by Sarkisov [55, 56]; a variant of this model would consider a distribution of the gap widths. Alternatively, as has been recently done by Wang and co-workers some spherical cavities of a mesoporous range are introduced into the model [28]. In both cases, this makes the model much more challenging from the computational point of view.

Finally, there is another technical challenge to a more systematic study on a larger number of systems. Standard GCMC simulations of water adsorption in carbons are very long, because of the very low acceptance ratio for insertions and deletions and it may take up to 1500 CPU hours (two months) to produce a single point on the adsorption isotherm. This is not surprising as conventional methods are based on a single molecule randomly added or removed from the system, while in reality these processes crucially depend on the formation of the hydrogen bond and fluctuation of the whole water cluster (see molecular dynamics visualizations of a single water molecule joining a water cluster stabilized between two carbon sheets). Hence, more comprehensive studies of water adsorption problems cannot be contemplated without developing more sophisticated coupled cluster-biased and orientation biased MC schemes.

Acknowledgements

We would like to thank Prof. Katsumi Kaneko and Prof. Matthias Thommes for useful discussions and suggestions concerning adsorption of water in activated carbons. We would like to thank Prof. Angel Linares-Solano and Prof. Peter Carrott for kindly providing the samples of Maxsorb. We would like to thank Prof. Christopher Hall for providing free access to the Aquadyne system. The University of Edinburgh, Energy Technology Partnership and Process System Enterprise are gratefully acknowledged for funding the experimental part of the current work. This work has made use of the resources provided by the Edinburgh Compute and Data Facility (ECDF) (http://www.ecdf.ed.ac.uk/).

References

[1] J.K. Brennan, T.J. Bandosz, K.T. Thomson, K.E. Gubbins, Water in porous carbons, Colloids and Surfaces A: Physicochemical and Engineering Aspects 187–188(0) (2001) 539-568.

[2] V.T. Nguyen, T. Horikawa, D.D. Do, D. Nicholson, Water as a potential molecular probe for functional groups on carbon surfaces, Carbon 67 (2014) 72-78.

[3] D.D. Do, D. Nicholson, Characterization of oxygen functional groups on carbon surfaces with water and methanol adsorption Yonghong Zeng a, Luisa Prasetyo a, Van T. Nguyen a, Toshihide Horikawa b, Carbon 81(1) (2015) 447-457.

[4] N. Klomkliang, R. Kaewmanee, S. Saimoey, S. Intarayothya, D.D. Do, D. Nicholson, Adsorption of water and methanol on highly graphitized thermal carbon black: The effects of functional group and temperature on the isosteric heat at low loadings, Carbon 99 (2016) 361-369.

[5] M. Thommes, C. Morlay, R. Ahmad, J.P. Joly, Assessing surface chemistry and pore structure of active carbons by a combination of physisorption (H2O, Ar, N2, CO2), XPS and TPD-MS, Adsorption 17(3) (2011) 653.

[6] M. Thommes, J. Morell, K.A. Cychosz, M. Fröba, Combining Nitrogen, Argon, and Water Adsorption for Advanced Characterization of Ordered Mesoporous Carbons (CMKs) and Periodic Mesoporous Organosilicas (PMOs), Langmuir 29(48) (2013) 14893-14902.

[7] L.F. Velasco, R. Guillet-Nicolas, G. Dobos, M. Thommes, P. Lodewyckx, Towards a better understanding of water adsorption hysteresis in activated carbons by scanning isotherms, Carbon 96 (2016) 753-758.

[8] E. Di Biase, L. Sarkisov, Systematic development of predictive molecular models of high surface area activated carbons for adsorption applications, Carbon 64 (2013) 262-280.

[9] E. Di Biase, L. Sarkisov, Molecular simulation of multi-component adsorption processes related to carbon capture in a high surface area, disordered activated carbon, Carbon 94 (2015) 27-40.

[10] M. Jorge, N.A. Seaton, Predicting adsorption of water/organic mixtures using molecular simulation, AIChE Journal 49(8) (2003) 2059-2070.

[11] T.J.B. Bandosz, M.J.; Gubbins, K.E.; Hattori, Y.; Iiyama, T.; Kaneko, K.; Picunik, J.; Thomson, K.T., in: L.R. Radovic (Ed.), Chemistry and Physics of Carbon, Mercel Dekker, New York, 2003, pp. 41-228.

[12] B. Smit, T.L.M. Maesen, Molecular Simulations of Zeolites: Adsorption, Diffusion, and Shape Selectivity, Chemical Reviews 108(10) (2008) 4125-4184.

[13] P. Bai, M. Tsapatsis, J.I. Siepmann, TraPPE-zeo: Transferable Potentials for Phase Equilibria Force Field for All-Silica Zeolites, The Journal of Physical Chemistry C 117(46) (2013) 24375-24387.

[14] A. Martin-Calvo, J.J. Gutierrez-Sevillano, J.B. Parra, C.O. Ania, S. Calero, Transferable force fields for adsorption of small gases in zeolites, Physical Chemistry Chemical Physics 17(37) (2015) 24048-24055.

[15] C. Vega, J.L.F. Abascal, Simulating water with rigid non-polarizable models: a general perspective, Physical Chemistry Chemical Physics 13(44) (2011) 19663-19688.

[16] G.A. Cisneros, K.T. Wikfeldt, L. Ojamäe, J. Lu, Y. Xu, H. Torabifard, A.P. Bartók, G. Csányi, V. Molinero, F. Paesani, Modeling Molecular Interactions in Water: From Pairwise to Many-Body Potential Energy Functions, Chemical Reviews 116(13) (2016) 7501-7528.

[17] C.E. Ramachandran, S. Chempath, L.J. Broadbelt, R.Q. Snurr, Water adsorption in hydrophobic nanopores: Monte Carlo simulations of water in silicalite, Microporous and Mesoporous Materials 90(1–3) (2006) 293-298.

[18] E.A. Müller, L.F. Rull, L.F. Vega, K.E. Gubbins, Adsorption of Water on Activated Carbons: A Molecular Simulation Study, The Journal of Physical Chemistry 100(4) (1996) 1189-1196.

[19] C.L. McCallum, T.J. Bandosz, S.C. McGrother, E.A. Müller, K.E. Gubbins, A Molecular Model for Adsorption of Water on Activated Carbon: Comparison of Simulation and Experiment, Langmuir 15(2) (1998) 533-544.

[20] E.A. Müller, K.E. Gubbins, Molecular simulation study of hydrophilic and hydrophobic behavior of activated carbon surfaces, Carbon 36(10) (1998) 1433-1438.

[21] T. Ohba, H. Kanoh, K. Kaneko, Water Cluster Growth in Hydrophobic Solid Nanospaces, Chemistry – A European Journal 11(17) (2005) 4890-4894.

[22] T. Ohba, K. Kaneko, Surface oxygen-dependent water cluster growth in carbon nanospaces with GCMC simulation-aided in situ SAXS, Journal of Physical Chemistry C 111(17) (2007) 6207-6214.

[23] A.H. Farmahini, G. Opletal, S.K. Bhatia, Structural Modelling of Silicon Carbide-Derived Nanoporous Carbon by Hybrid Reverse Monte Carlo Simulation, Journal of Physical Chemistry C 117(27) (2013) 14081-14094.

[24] E.I. Segarra, E.D. Glandt, Model microporous carbons: microstructure, surface polarity and gas adsorption, Chemical Engineering Science 49(17) (1994) 2953-2965.

[25] J.-C. Liu, P.A. Monson, Molecular Modeling of Adsorption in Activated Carbon: Comparison of Monte Carlo Simulations with Experiment, Adsorption 11(1) (2005) 5-13.

[26] J.C. Liu, P.A. Monson, Monte Carlo Simulation Study of Water Adsorption in Activated Carbon, Industrial & Engineering Chemistry Research 45(16) (2006) 5649-5656.

[27] K.V. Kumar, E.A. Müller, F. Rodríguez-Reinoso, Effect of Pore Morphology on the Adsorption of Methane/Hydrogen Mixtures on Carbon Micropores, The Journal of Physical Chemistry C 116(21) (2012) 11820-11829.

[28] S. Wang, L. Lu, D. Wu, X. Lu, W. Cao, T. Yang, Y. Zhu, Molecular Simulation Study of the Adsorption and Diffusion of a Mixture of CO2/CH4 in Activated Carbon: Effect of Textural Properties and Surface Chemistry, Journal of Chemical & Engineering Data 61(12) (2016) 4139-4147.

[29] S. Furmaniak, P. Kowalczyk, A.P. Terzyk, P.A. Gauden, P.J.F. Harris, Synergetic effect of carbon nanopore size and surface oxidation on CO2 capture from CO2/CH4 mixtures, Journal of Colloid and Interface Science 397(0) (2013) 144-153.

[30] Y. Huang, F.S. Cannon, J.K. Watson, B. Reznik, J.P. Mathews, Activated carbon efficient atomistic model construction that depicts experimentally-determined characteristics, Carbon 83(0) (2015) 1-14.

[31] X. Lu, D. Jin, S. Wei, M. Zhang, Q. Zhu, X. Shi, Z. Deng, W. Guo, W. Shen, Competitive adsorption of a binary CO2-CH4 mixture in nanoporous carbons: effects of edge-functionalization, Nanoscale 7(3) (2015) 1002-1012.

[32] P.I. Ravikovitch, A.V. Neimark, Density Functional Theory Model of Adsorption on Amorphous and Microporous Silica Materials, Langmuir 22(26) (2006) 11171-11179.

[33] T. Otowa, R. Tanibata, M. Itoh, Production and adsorption characteristics of MAXSORB: High-surface-area active carbon, Gas Separation & Purification 7(4) (1993) 241-245.

[34] J. Landers, G.Y. Gor, A.V. Neimark, Density functional theory methods for characterization of porous materials, Colloids and Surfaces A: Physicochemical and Engineering Aspects 437 (2013) 3-32.

[35] L. Sarkisov, A. Harrison, Computational structure characterisation tools in application to ordered and disordered porous materials, Molecular Simulation 37(15) (2011) 1248-1257.

[36] A. Gupta, S. Chempath, M.J. Sanborn, L.A. Clark, R.Q. Snurr, Object-oriented Programming Paradigms for Molecular Modeling, Molecular Simulation 29(1) (2003) 29-46.

[37] A. Striolo, A.A. Chialvo, P.T. Cummings, K.E. Gubbins, Water Adsorption in Carbon-Slit Nanopores, Langmuir 19(20) (2003) 8583-8591.

[38] A. Striolo, A.A. Chialvo, K.E. Gubbins, P.T. Cummings, Water in carbon nanotubes: Adsorption isotherms and thermodynamic properties from molecular simulation, The Journal of Chemical Physics 122(23) (2005) 234712.

[39] A. Striolo, P.K. Naicker, A.A. Chialvo, P.T. Cummings, K.E. Gubbins, Simulated Water Adsorption Isotherms in Hydrophilic and Hydrophobic Cylindrical Nanopores, Adsorption 11(1) (2005) 397-401.

[40] M.J. Abraham, T. Murtola, R. Schulz, S. Páll, J.C. Smith, B. Hess, E. Lindahl, GROMACS: High performance molecular simulations through multi-level parallelism from laptops to supercomputers, SoftwareX 1–2 (2015) 19-25.

[41] C.M. Tenney, C.M. Lastoskie, Molecular simulation of carbon dioxide in chemically and structurally heterogeneous porous carbons, Environmental Progress 25(4) (2006) 343.

[42] D.B. Axel, A new mixing of Hartree--Fock and local density-functional theories, The Journal of Chemical Physics 98(2) (1993) 1372-1377.

[43] C.M. Breneman, K.B. Wiberg, Determining atom-centered monopoles from molecular electrostatic potentials. The need for high sampling density in formamide conformational analysis, Journal of Computational Chemistry 11(3) (1990) 361-373.

[44] M.J.T. Frisch, G. W.; Schlegel, H. B.; Scuseria, G. E.; Robb, M. A.; Cheeseman, J. R.; Scalmani, G.; Barone, V.; Mennucci, B.; Petersson, G. A.; Nakatsuji, H.; Caricato, M.; Li, X.; Hratchian, H. P.; Izmaylov, A. F.; Bloino, J.; Zheng, G.; Sonnenberg, J. L.; Hada, M.; Ehara, M.; Toyota, K.; Fukuda, R.; Hasegawa, J.; Ishida, M.; Nakajima, T.; Honda, Y.; Kitao, O.; Nakai, H.; Vreven, T.; Montgomery, Jr., J. A.; Peralta, J. E.; Ogliaro, F.; Bearpark, M.; Heyd, J. J.; Brothers, E.; Kudin, K. N.; Staroverov, V. N.; Kobayashi, R.; Normand, J.; Raghavachari, K.; Rendell, A.; Burant, J. C.; Iyengar, S. S.; Tomasi, J.; Cossi, M.; Rega, N.;

Millam, J. M.; Klene, M.; Knox, J. E.; Cross, J. B.; Bakken, V.; Adamo, C.; Jaramillo, J.; Gomperts, R.; Stratmann, R. E.; Yazyev, O.; Austin, A. J.; Cammi, R.; Pomelli, C.; Ochterski, J. W.; Martin, R. L.; Morokuma, K.; Zakrzewski, V. G.; Voth, G. A.; Salvador, P.; Dannenberg, J. J.; Dapprich, S.; Daniels, A. D.; Farkas, Ö.; Foresman, J. B.; Ortiz, J. V.; Cioslowski, J.; Fox, D. J. , Gaussian 09, Revision A.1, 2009.

[45] W.L. Jorgensen, J. Chandrasekhar, J.D. Madura, R.W. Impey, M.L. Klein, Comparison of simple potential functions for simulating liquid water, Journal of Chemical Physics 79(2) (1983) 926-935.

[46] J.W. Essam, Phase transitions and critical phenomena, in: C. Domb, and Green, M. S. (Ed.), Phase transitions and critical phenomena, Academic Press, New York, 1972, p. 197.

[47] J. Miyawaki, T. Kanda, K. Kaneko, Hysteresis-associated pressure-shift-induced water adsorption in carbon micropores, Langmuir 17(3) (2001) 664-669.

[48] A.H. Farmahini, D.S. Sholl, S.K. Bhatia, Fluorinated Carbide-Derived Carbon: More Hydrophilic, Yet Apparently More Hydrophobic, Journal of the American Chemical Society 137(18) (2015) 5969-5979.

[49] A.C. Mitropoulos, E.P. Favvas, K.L. Stefanopoulos, E.F. Vansant, Scanning of Adsorption Hysteresis In Situ with Small Angle X-Ray Scattering, PLOS ONE 11(10) (2016) e0164636.

[50] D.Y. Dubov, A.A. Vostrikov, Dipole moment of a small water cluster. The effect of size, temperature, and electric field, JETP Letters 92(1) (2010) 28-32.

[51] S.Y. Qi, K.J. Hay, M.J. Rood, M.P. Cal, Equilibrium and heat of adsorption for water vapor and activated carbon, Journal of Environmental Engineering-Asce 126(3) (2000) 267-271.

[52] T.X. Nguyen, S.K. Bhatia, How Water Adsorbs in Hydrophobic Nanospaces, Journal of Physical Chemistry C 115(33) (2011) 16606-16612.

[53] D.D. Do, H.D. Do, A model for water adsorption in activated carbon, Carbon 38(5) (2000) 767-773.

[54] C. Vega, J.L.F. Abascal, I. Nezbeda, Vapor-liquid equilibria from the triple point up to the critical point for the new generation of TIP4P-like models: TIP4P/Ew, TIP4P/2005, and TIP4P/ice, The Journal of Chemical Physics 125(3) (2006) 034503.

[55] L. Sarkisov, Molecular simulation of perfluorohexane adsorption in BAM-P109 activated carbon, Adsorption Science & Technology 34(1) (2016) 42-63.

[56] L. Sarkisov, Molecular simulation of low temperature argon adsorption in several models of IRMOF-1 with defects and structural disorder, Dalton Transactions 45(10) (2016) 4203-4212.